Applied Catalysis B: Environmental 254 (2019) 7–14

Contents lists available at ScienceDirect

Applied Catalysis B: Environmental

journal homepage: www.elsevier.com/locate/apcatb

Photocatalytic water splitting over Pt-loaded TiO_2 (Pt/TiO_2) catalysts prepared by the polygonal barrel-sputtering method

Keisuke Matsubara, Mitsuhiro Inoue, Hidehisa Hagiwara, Takayuki Abe*

Hydrogen Isotope Research Center, Organization for Promotion of Research, University of Toyama, 3190 Gofuku, Toyama, 930-8555, Japan

ARTICLE INFO

Keywords:
Photocatalytic water splitting
H_2 production
Pt/TiO_2 photocatalyst
Polygonal barrel-sputtering method
Pt nanoparticle

ABSTRACT

Pt-loaded TiO_2 (Pt/TiO_2) catalysts for photocatalytic water splitting were prepared by the polygonal barrel-sputtering method. The results showed that the evolution rates of H_2 and O_2 gases for our Pt/TiO_2 catalysts were ca. 5–10 times of those prepared by a conventional photodeposition method. The molar ratios of H_2 versus O_2 were close to be 2, revealing that the stoichiometric water decomposition occurred. The characterizations of the prepared samples implied that the smaller Pt nanoparticles were highly dispersed on the TiO_2 particles by the polygonal barrel-sputtering method. The deposition of the smaller Pt particles increased the Pt surface areas, which can improve the water splitting activities. In addition, the particles deposited by the sputtering method were electron-deficient Pt metals that can enhance the water splitting reaction, whereas those by the photodeposition method were electron-rich Pt metals that reduce the effectiveness of the photocatalytic reaction. These different electron states would play an important role in the remarkable differences in the water splitting activities between the Pt/TiO_2 catalysts. Consequently, the polygonal barrel-sputtering method is useful for preparing photocatalysts with the high water splitting activities.

1. Introduction

Hydrogen (H_2) is currently attracts considerable attentions as a renewable energy [1]. There are several methods for producing H_2 gas [2–15]. Among the available methods, photocatalytic water splitting is an environmentally friendly H_2 producing method, because of no emission of greenhouse gases such as carbon dioxide (CO_2) [6-15].

In the photocatalytic water splitting, various kinds of semiconductor particles have been used [6–12]. When the semiconductors are irradiated, the holes and electrons are generated, leading to the following water splitting reactions [8]:

$$H_2O + 2\,h^+ \rightarrow 1/2O_2 + 2H^+ \quad (1)$$

$$H^+ + 2e^- \rightarrow H_2. \quad (2)$$

However, the water splitting over the semiconductors is difficult, since the holes and electrons generated recombine very easily [10].

On the other hand, nanoparticles such as metals and metal oxides can capture electrons generated from the semiconductors [12,13]. Therefore, numerous photocatalysts have been prepared by depositing nanoparticles on semiconductors in order to exclude the recombination of photoholes and electrons [12–24]. However, the water splitting performances of the current photocatalysts must be further improved to achieve the highly efficient H_2 production.

It has been reported that the high dispersion of smaller nanoparticles on the semiconductors makes it possible to improve the water splitting performances of the catalysts [22,23]. Based on this finding, we focused our attention on our original particle surface modification process called as the “polygonal barrel-sputtering method” [25–39]. This method is based on a sputtering technique, in which nucleation and particle growth of the sputtered materials reportedly lead to the deposition of nanoparticles on supports [40]. For our method, the formation of the nanoparticles occurs on the particle surfaces used as the supports [39]. In addition, this original sputtering method contains no heating procedure, allowing the high dispersion of small nanoparticles of metals [32,34,35,38], metal alloys [31,33,36,37], or metal oxides [36]. In this study, Pt-loaded TiO_2 (Pt/TiO_2) catalysts, which are well-known as a common photocatalyst for water splitting [14–19], were prepared by the polygonal-barrel sputtering method, and their photocatalytic water splitting performances were examined.

2. Experimental

2.1. Preparation of Pt/TiO_2 samples

The polygonal barrel-sputtering apparatus used for preparing Pt/

* Corresponding author.
E-mail address: tabe@ctg.u-toyama.ac.jp (T. Abe).

https://doi.org/10.1016/j.apcatb.2019.04.075
Received 25 February 2019; Received in revised form 15 April 2019; Accepted 21 April 2019
Available online 22 April 2019
0926-3373/ © 2019 Elsevier B.V. All rights reserved.

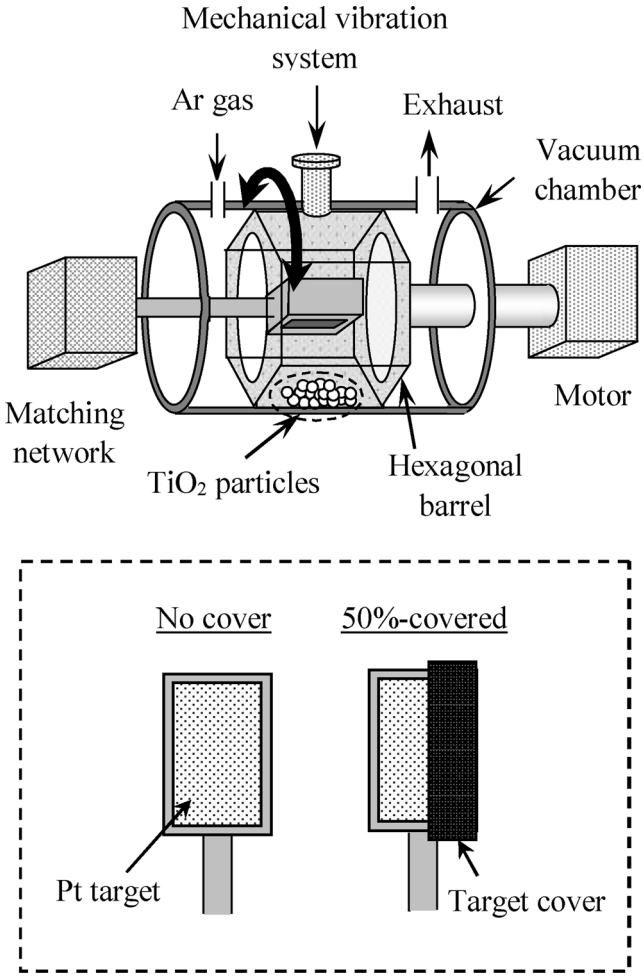

Fig. 1. Schematic diagram of the polygonal barrel-sputtering system.

TiO_2 samples is shown in Fig. 1 [25–39]. This apparatus is composed of a vacuum chamber including a hexagonal barrel, in which a powdered support is introduced. A Pt plate (99.99% purity, W 50 mm × l 100 mm) was used as the target for sputtering. TiO_2 particles (mean primary particle size, 21 nm, P25; Nippon Aerosil) used as the support were heated at 180 °C to prevent aggregation of the particles by water during preparation in advance [31,35]. The Pt/TiO_2 sample was prepared as follows [25–39]. The pre-heated TiO_2 powder of 2 g was introduced into the hexagonal barrel and the barrel was placed in the vacuum chamber. The vacuum chamber was then carefully evacuated using a rotary pump and a diffusion pump. After the pressure was decreased to less than 8×10^{-4} Pa, Ar gas (purity: 99.9999%) was slowly introduced into the chamber. Subsequently, sputtering was performed at an Ar gas pressure of 0.8 Pa without heating. An AC power of 25 W was supplied by RF power generation (13.56 MHz) to highly disperse the small Pt nanoparticles on the surfaces of the TiO_2 particles. During the sputtering, to fragment the secondary particles of the TiO_2 into the primary particles, and then stir them, the hexagonal barrel was oscillated (intervals of 14 s and amplitude of ± 75°) and vibrated mechanically. The amount of Pt deposited was controlled by changing the sputtering time between 5–15 min (see Table 1). When the samples with the Pt deposition amount of 0.05 and 0.10 wt.% were prepared, a half of the Pt target plate was covered with a stainless plate, as shown in Fig. 1. After sputtering, N_2 gas was gradually introduced to the atmospheric pressure, at which the prepared samples could be extracted. Hereafter, the samples prepared by the polygonal barrel-sputtering method are denoted as (BS)-Pt/TiO_2.

Pt/TiO_2 samples used as references were prepared by a conventional photodeposition method using a closed gas-circulating system through the following procedure [16]. The TiO_2 of 1 g and $H_2PtCl_6{\cdot}6H_2O$ (> 98.5% purity, Kanto Chemical) of a certain weight were uniformly mixed in a Pyrex glass-photoreactor including 1050 ml of aqueous methanol solution (10 vol.%) by stirring the solution at 500 rpm using a magnetic stirrer (MS 500D; Yamato). After the suspension was deaerated with Ar gas, the irradiation was conducted for 12 h using a 400 W-high-pressure Hg lamp (HL400B-8; Sen Tokushu Kogen) as the light source. During irradiation, the suspension was stirred at 500 rpm and the temperature was kept at 25 °C by circulating water through a cylindrical Pyrex jacket around the light source. The Pt/TiO_2 samples obtained by the above procedure are denoted as (PD)-Pt/TiO_2.

Table 1
Sputtering conditions and Pt deposited amount of (BS)-Pt/TiO_2 samples.

Sputtering conditions[a,b]		Pt deposition amount[c] / wt. %
Covered area of Pt target	Sputtering time / min	
50%	5	0.05
50%	10	0.10
No cover	15	0.19

[a] The other sputtering conditions were Ar gas pressure of 0.8 Pa and AC power of 25 W.
[b] Sputtering was conducted without heating.
[c] The Pt deposited amounts were determined by ICP-AES.

2.2. Photocatalytic water splitting on Pt/TiO_2 [15–17]

Photocatalytic water splitting over the Pt/TiO_2 samples was performed in the same photoreactor as that used for the (PD)-Pt/TiO_2 preparation. The UV light irradiation was carried out while a Pt/TiO_2 sample of 0.3 g was suspended in 1050 ml of ion exchanged water (stirring velocity: 500 rpm). The reactant gas (1 ml) was periodically collected by a gas sampler, and it was analyzed by a gas chromatograph (GC2014; Shimadzu) equipped with a thermal conductivity detector (TCD) and a molecular sieve 5 A column (GL Science). In the gas chromatography, Ar gas used as the carrier gas was supplied at a rate of 50 sccm. The temperatures of the gas injector, column, and detector were set at 170, 150, and 170 °C, respectively.

2.3. Characterization of the prepared Pt/TiO_2 samples

The amounts of Pt deposited in the prepared samples were estimated by an inductively coupled plasma-atomic emission spectroscopy (ICP-AES: Optima 7300DV; PerkinElmer). The solutions for the ICP measurement were prepared by heating the Pt/TiO_2 sample (100 mg) in aqua regia (3 ml) for 1 h, followed by diluting the obtained solution to 100 ml with Millipore water. The microscopic properties of the Pt/TiO_2 samples were evaluated by transmission electron microscopy (TEM: JEM-2100; JEOL) at the accelerating voltage of 200 kV. The size distributions of the deposited Pt particles were obtained by directly measuring the size of more than 150 randomly chosen particles from the magnified TEM images. The prepared samples were also characterized by an X-ray diffraction analysis (XRD: Philips; PW1825/00) with Cu Kα radiation operating at 40 kV and 30 mA. The optical properties of the Pt/TiO_2 samples were examined by an ultraviolet-visible (UV-VIS) spectrometer (V-560i RM; JASCO). The electron state of the deposited Pt was assessed by an X-ray photoelectron spectroscopy (XPS: ESCALAB 250X; Thermo Fisher Scientific) which was performed at 25 W using monochromatized Al Kα excitation. The obtained spectra were referenced with respect to C1s core level of a bonding energy of 284.8 eV [41].

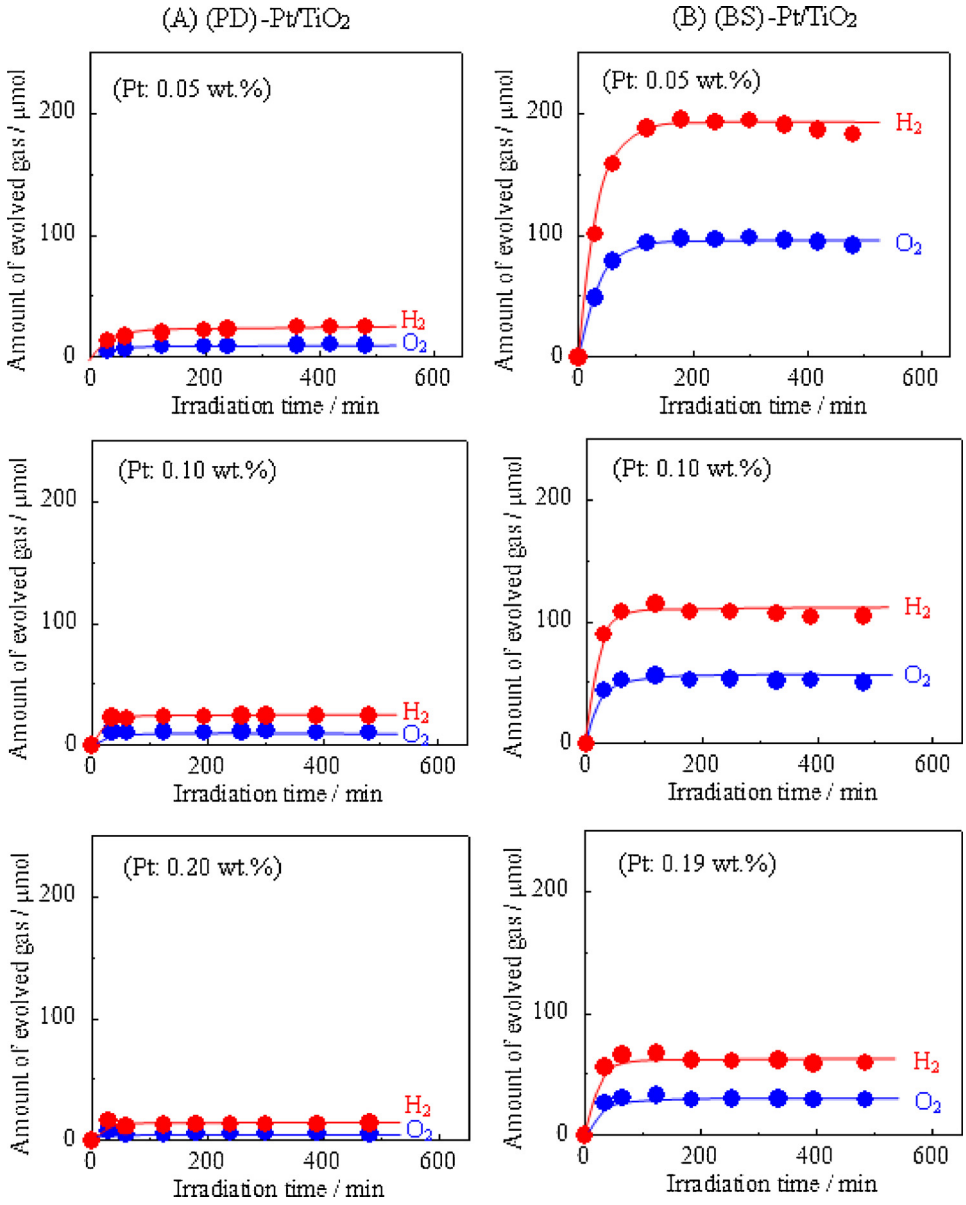

Fig. 2. Amounts of H_2 and O_2 gases generated by photocatalytic water splitting over (A) (PD)-Pt/TiO_2 and (B) (BS)-Pt/TiO_2 samples versus UV irradiation time.

Table 2
Evolution rates of H_2 and O_2 gases and Pt surface areas of Pt/TiO_2 samples used in photocatalytic water splitting.

Amount of deposited Pt / wt.%	Gas evolution rate / μmol h^{-1}			Pt surface area (SA_{Pt})[a] / cm^2	Turnover frequency / × 10^{-2} s^{-1}	
	H_2	O_2	H_2/O_2 molar ratio		H_2	O^2
– (PD)-Pt/TiO_2 –						
0.05	17.1	7.3	2.4	144.7	4.80	2.05
0.10	22.0	10.5	2.1	190.7	4.70	2.24
0.20	11.2	4.6	2.4	349.7	1.30	0.53
– (BS)-Pt/TiO_2 –						
0.05	157.7	78.6	2.0	246.8	25.44	12.84
0.10	107.8	51.7	2.1	466.2	9.36	4.49
0.19	59.6	27.8	2.1	885.8	2.71	1.27

[a] The data were determined from Eq. (3).

3. Results and discussion

3.1. Water splitting performances of the prepared Pt/TiO_2 catalysts

The photocatalytic water splitting over the Pt/TiO_2 samples was carried out in the ion exchanged water without any electrolytes. The H_2 and O_2 gases were evolved for all the samples, which might be attributed to the partial irradiation of the UV light from the top of the suspension [16,19]. Fig. 2 shows the amounts of the evolved H_2 and O_2 gases versus the irradiation time. Over (PD)-Pt/TiO_2, the amounts of the H_2 and O_2 gases gradually increased until the irradiation time of 60 min (Fig. 2(A)). After 60 min, the gas evolution was suppressed. The factors inducing this trend are considered to be the increase in the pressure in the reactor due to the closed system [15] and the effect of the reverse reaction ($H_2 + 1/2O_2 \rightarrow H_2O$), as described later in this paper, although the details are uncertain. Similar trends of the gas evolutions were observed for the (BS)-Pt/TiO_2 samples, as shown in Fig. 2(B). However, the evolution amounts of H_2 and O_2 for (BS)-Pt/TiO_2 were significantly larger than those for (PD)-Pt/TiO_2.

From the data at 60 min in Fig. 2, the evolution rates of H_2 and O_2

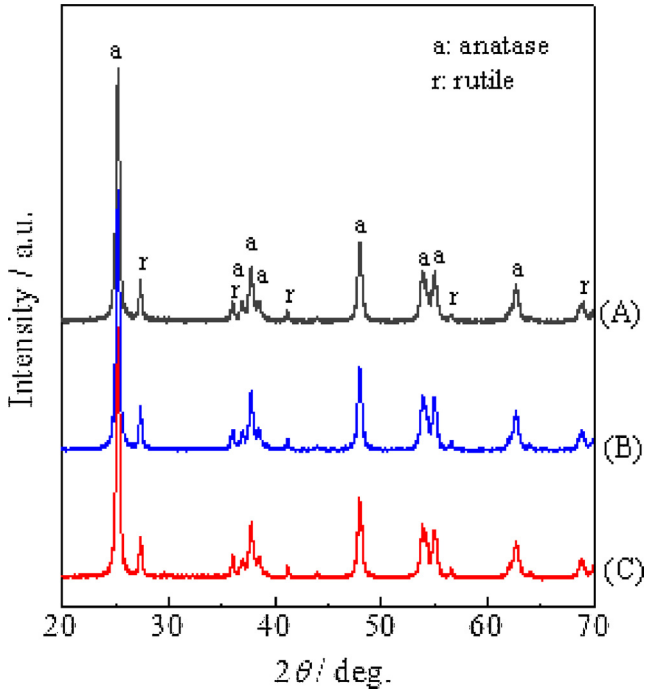

Fig. 3. XRD patterns of (A) as-received TiO_2, (B) (PD)-Pt/TiO_2, and (C) (BS)-Pt/TiO_2. The Pt deposition amounts for the Pt/TiO_2 samples were 0.05 wt.%.

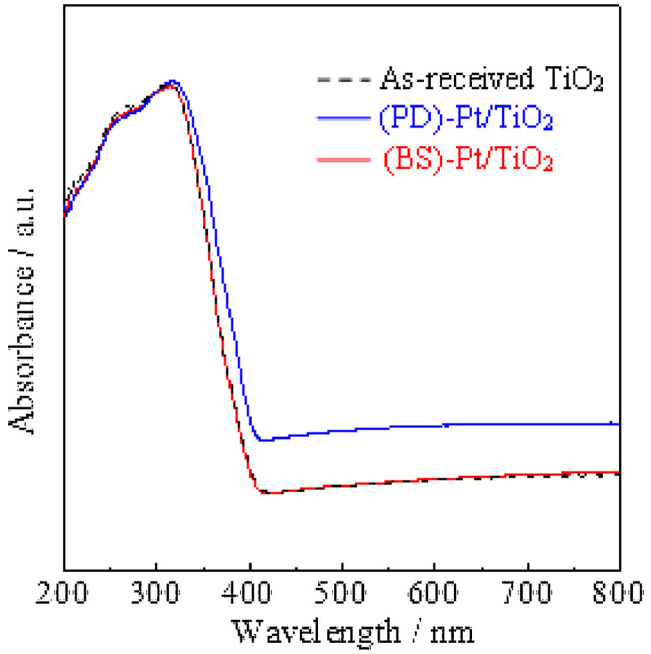

Fig. 4. UV-VIS spectra of as-received TiO_2, (PD)-Pt/TiO_2, and (BS)-Pt/TiO_2. The Pt deposition amounts for the Pt/TiO_2 samples were 0.05 wt.%.

were determined. The obtained results are listed in Table 2. For (PD)-Pt/TiO_2, the evolution rates of H_2 and O_2 were 11.2–22.0 and 4.6–10.5 μmol h^{-1}, respectively. In the case of (BS)-Pt/TiO_2, the gas evolution rates (H_2: 59.6–157.7 μmol h^{-1}, O_2: 27.8–78.6 μmol h^{-1}) were ca. 5–10 times greater than those for (PD)-Pt/TiO_2 with the similar Pt deposition amounts. The water splitting activity of Pt/TiO_2 was apparently improved by the polygonal barrel-sputtering method. It should be noted that the molar ratios of H_2 versus O_2 (H_2/O_2 molar ratios) in Table 2 were close to 2 for all the samples, indicating that the gas evolutions occurred via the stoichiometric water decomposition of $H_2O \rightarrow H_2 + 1/2O_2$.

3.2. Factors inducing high water splitting activity of (BS)-Pt/TiO_2

To investigate the factors of the high water splitting activities, the physical properties of the prepared samples were evaluated. Fig. 3 shows the XRD patterns of (A) as-received TiO_2, (B) (PD)-Pt/TiO_2, and (C) (BS)-Pt/TiO_2. Because of the small amount of the Pt deposited (= 0.05 wt.%), no peaks characteristic of Pt were observed for both Pt/TiO_2 samples. All the diffraction peaks in the Pt/TiO_2 samples agreed with the signals of the as-received TiO_2 which were assigned to those of the anatase and rutile structures [42,43]. Thus, the crystal structure of TiO_2 used as the supports did not change by the Pt deposition.

The UV-VIS spectra of the same samples are shown in Fig. 4. For (PD)-Pt/TiO_2, an absorption in the visible light region (> 400 nm) increased due to the fact that the incident photon frequency is resonant with the collective excitations of the conduction electrons of the deposited Pt [41]. Such absorption was not observed for (BS)-Pt/TiO_2, despite the identical Pt deposition amount to that for (PD)-Pt/TiO_2. The different absorption in the visible light region between (PD)-Pt/TiO_2 and (BS)-Pt/TiO_2 may concern with the sizes of the Pt particles in each sample, as described latter. It is noted that a strong absorption in the UV region (< 400 nm) observed for (BS)-Pt/TiO_2 was similar to those for both (PD)-Pt/TiO_2 and the TiO_2 support, suggesting that the optical properties of the Pt/TiO_2 samples did not affect the difference in their photocatalytic water splitting activities.

Fig. 5(A) and (B) show typical TEM images of (PD)-Pt/TiO_2 and (BS)-Pt/TiO_2, respectively. For all the samples, Pt nanoparticles shown as black dots were observed on the gray TiO_2 support background. As compared to (PD)-Pt/TiO_2, the Pt particles were highly dispersed in (BS)-Pt/TiO_2. The size distributions of Pt particles in each sample are also represented in Fig. 5. For (PD)-Pt/TiO_2, the Pt particles ranged from 1.0–4.6 nm at the Pt deposition amount of 0.05 wt.%. The particle size distribution for (PD)-Pt/TiO_2 became wider by increasing the Pt deposition amounts to 0.10 and 0.20 wt. %. The center of the particle sizes also shifted to the larger size with the increase in the Pt deposition amount. From these size distributions, the mean particle sizes were estimated to be 2.9 nm (Pt: 0.05 wt.%), 4.4 nm (Pt: 0.10 wt.%), and 4.8 nm (Pt: 0.20 wt.%). As for (BS)-Pt/TiO_2, the Pt particles had similar sizes of 0.8–3.0 nm for all the samples. The mean particle sizes were ca. 1.8 nm, which was smaller than those of (PD)-Pt/TiO_2.

When the shapes of the deposited Pt particles are supposed to be sphere, the Pt surface areas of the samples used in the photocatalytic reactions (SA_{Pt}, in cm^2) can be calculated using the following equation [44,45]:

$$SA_{Pt} = (6000/\rho d \times 10^4) \times w/100 \times 0.3 \quad (3)$$

where ρ is the Pt density (21.45 g cm^{-3}), d and w are mean particle size of the deposited Pt obtained by TEM (in nm) and its deposition amount (in wt.%), respectively, and 0.3 is a weight of the Pt/TiO_2 sample used in the reaction. The SA_{Pt} values calculated from Eq. (3) are summarized in Table 2. The (BS)-Pt/TiO_2 samples with the Pt deposition amounts of 0.05, 0.10, and 0.19 wt.% gave the SA_{Pt} values of 246.8, 466.2, and 885.8 cm^2, respectively. These values were 1.7–2.5 times of those of the (PD)-Pt/TiO_2 samples with the similar Pt deposition amounts, which can contribute to the high water splitting activities of (BS)-Pt/TiO_2. However, the turnover frequencies of the H_2 and O_2 evolution for (BS)-Pt/TiO_2, which were semi-quantitatively estimated using the SA_{Pt} values and the atomic radius of Pt (1.39 Å), were 2.0–5.3 times larger than those for (PD)-Pt/TiO_2 (see Table 2). In addition, the turnover frequencies obtained for (BS)-Pt/TiO_2 decreased with the increasing Pt deposited amount. These results suggest that there were other factors affecting the water splitting activity of Pt/TiO_2.

The distances between the Pt particles were also estimated from the TEM images. As a result, the mean distances between the Pt particles deposited in (BS)-Pt/TiO_2 decreased from 8.4–6.1 and 5.3 nm as the Pt

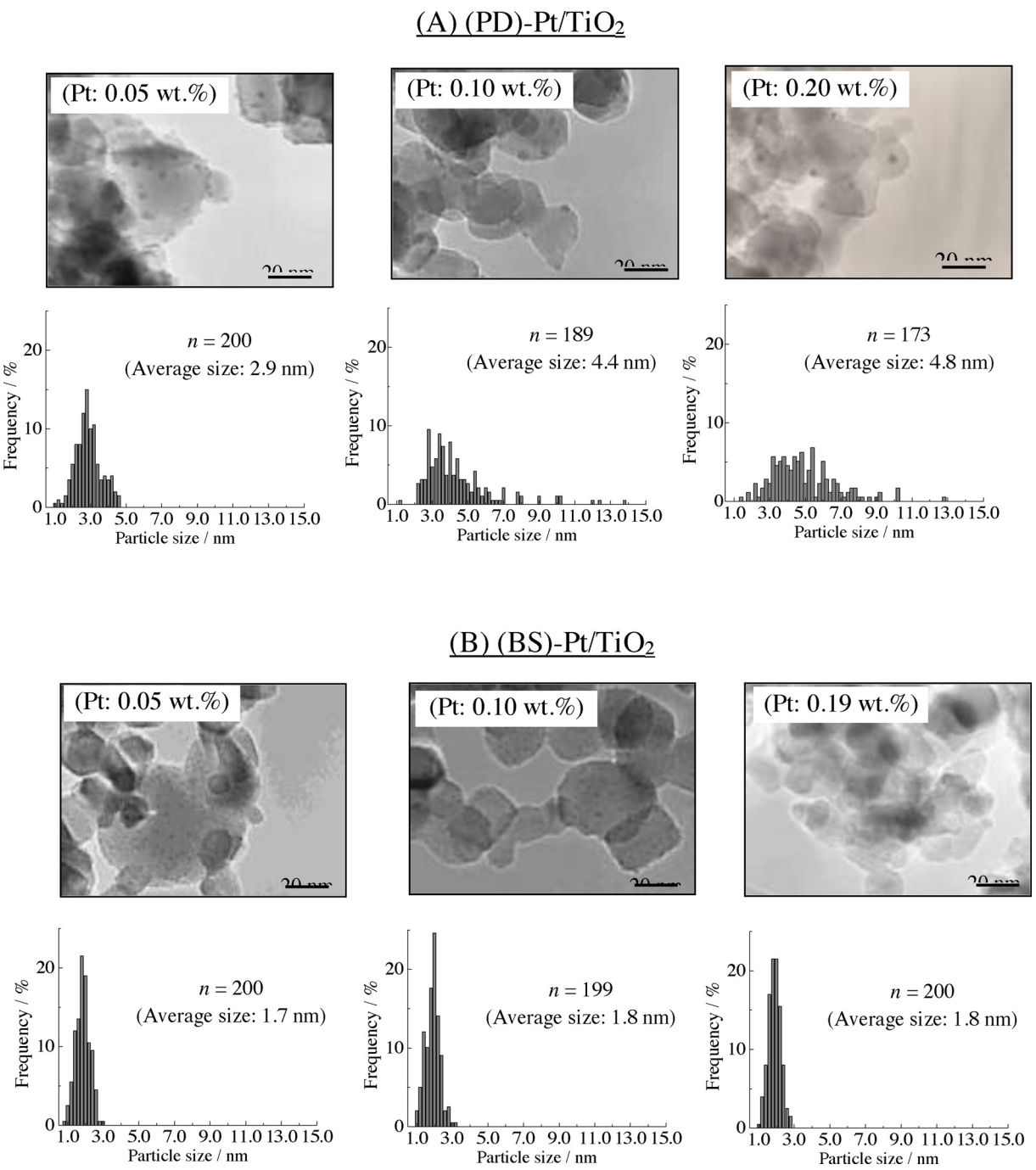

Fig. 5. Typical TEM images (accelerating voltage, 200 kV) and particle size distributions (*n*: number of particle counts) of (A) (PD)-Pt/TiO_2 and (B) (BS)-Pt/TiO_2 samples.

deposition amount was increased from 0.05 to 0.10 and 0.19 wt.%. For the water splitting reaction, the H_2 and O_2 generated tend to convert again into water on the Pt particles via a reaction of $H_2 + 1/2O_2 \rightarrow H_2O$ [17,18]. Indeed, even over (BS)-Pt/TiO_2 with the Pt deposition amount of 0.05 wt.%, the reverse reaction of $H_2 + 1/2O_2 \rightarrow H_2O$ occurred at the rates of H_2 = 14.1 μmol/h and O_2 = 7.8 μmol/h when the UV lump was turned off after the H_2 and O_2 evolution became steady-state. The frequency of this reverse reaction should increase by the approach of the Pt particles. Moreover, the reverse reaction might contribute to the suppression of the H_2 and O_2 evolution after 60 min. On the other hand, the decrease in the distances between the Pt particles also means the increase in the Pt coverage on the TiO_2 surfaces. This factor induces the inner filter effect, which suppresses the water splitting reaction [23]. Based on these factors, the difference in the turnover frequencies for (BS)-Pt/TiO_2 in Table 2 can be well explained by the Pt particle distances. However, for (PD)-Pt/TiO_2, the mean distance between the Pt particles was estimated to be 10.1 nm at the Pt deposition amount of 0.05 wt.%, which was longer than that of the (BS)-Pt/TiO_2 with the same Pt amount, despite the low water splitting activity. It is thereby considered that the distances between the Pt particles did not originally participate in the different water splitting activities between (BS)-Pt/TiO_2 and (PD)-Pt/TiO_2.

The electron states of the Pt deposited were examined by XPS. Fig. 6 shows the Pt4f spectra of the (PD)-Pt/TiO_2 and (BS)-Pt/TiO_2 samples. It is seen in the spectra of the (PD)-Pt/TiO_2 samples that two deconvoluted peaks corresponding to the $Pt4f_{7/2}$ and $Pt4f_{5/2}$ peaks were

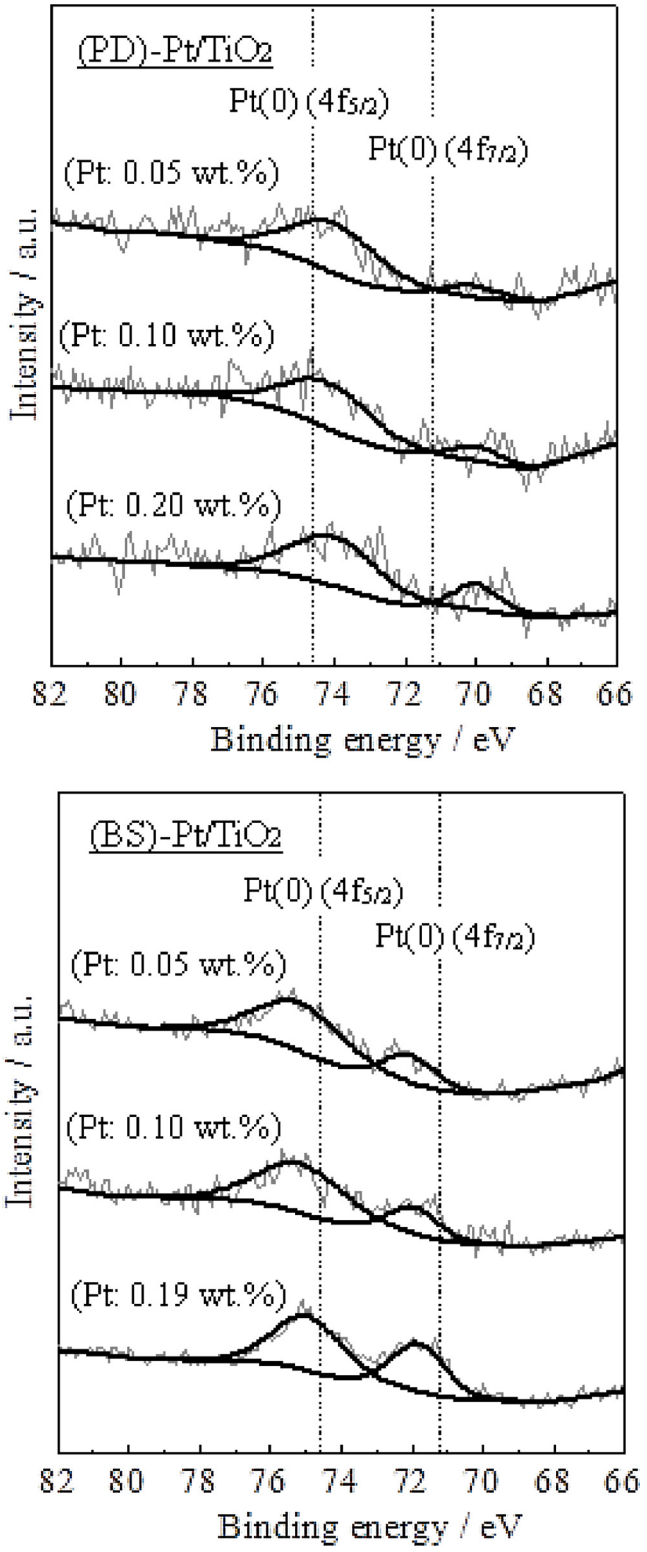

Fig. 6. Pt4f spectra of (PD)-Pt/TiO_2 and (BS)-Pt/TiO_2 obtained by XPS. The dashed lines show typical binding energies of $Pt4f_{5/2}$ and $Pt4f_{7/2}$ peaks for metallic Pt [43].

observed at 70.1 and 74.0 eV (Pt: 0.05 wt.%), 70.0 and 74.1 eV (Pt: 0.10 wt.%), and 70.0 and 74.0 eV (Pt: 0.20 wt.%). As compared to the reported peak positions of a metallic Pt expressed by dashed lines in this figure (71.2 and 74.6 eV [46]), the Pt4f peaks for (PD)-Pt/TiO_2 apparently shifted to the lower binding energies. The peak shifts to the lower biding energy indicate the deposition of the Pt metal particles with an electron-rich state [47,48]. For the photodeposition, defect sites ($TiO_{2-\delta}$) included in TiO_2 plays an important role as the active sites for the formation of the metal particles [48]: Ti^{3+} in $TiO_{2-\delta}$, which acts as the electron trap sites, leads to the electron transfer from TiO_2 to Pt, resulting in the deposition of the electron-rich Pt metal particles [47,48]. It has also been reported that the electron-rich Pt metals may repel electrons, which reduces the effectiveness of photocatalytic reaction [49]. This negative effect most likely contributed to the low water splitting activities of the (PD)-Pt/TiO_2 samples.

As for the (BS)-Pt/TiO_2 samples, the deconvoluted $Pt4f_{7/2}$ and $Pt4f_{5/2}$ peaks were observed at 72.1 and 75.1 eV (Pt: 0.05 wt.%), 72.0 and 75.1 eV (Pt: 0.10 wt.%), and 71.8 and 74.9 eV (Pt: 0.19 wt.%). The Pt4f peak positions for (BS)-Pt/TiO_2, as mentioned above, were higher than those of the metallic Pt, while those were lower than those reported for Pt(II) (72.8–73.1 and 76.3–76.4 eV [50]) and Pt(IV) (74.6–74.9 and 78.1–78.2 eV [50]). These results are completely different from those for (PD)-Pt/TiO_2 and show that the Pt particles in (BS)-Pt/TiO_2 were composed of the Pt metals with an electron-deficient that can enhance the electron collection [23,51,52]: this factor positively affects the photocatalytic reaction [23,51,52], which is probably induced by the initial state effects, e.g. charge transfer from metals to supports, lattice strain due to the small particle sizes, existence of many undercoodinated atoms, and so on [53,54]. In addition, similar peak shift was observed for (BS)-Pt/TiO_2 with Pt = 0.05 wt.% after the photoreaction, suggesting that the electron-deficient state of Pt was remained during the reaction. Consequently, the deposition of the electron-deficient Pt particles is most likely to originally contribute to the high water splitting activities of (BS)-Pt/TiO_2. It is emphasized that the XPS peaks of metals such as Au, Ag, Ni, Cu, and Pt have been reported to shift to the higher binding energies with the decrease in the particle sizes [53–58]. Especially, the study reported by Garbarino et al has shown that the significantly positive shifts of the Pt4f peaks were observed at the particle sizes of less than 3 nm [54]. Based on these reports, the deposition of the electron-deficient Pt particles for (BS)-Pt/TiO_2 may be attributed to the Pt particle sizes of less than 3 nm, as described in Fig. 5.

4. Conclusions

In this study, we prepared the Pt/TiO_2 catalysts by the polygonal barrel-sputtering method and their photocatalytic water splitting performances were compared to those prepared by the conventional photodeposition method. The obtained results are summarized as follows.

(1) For the photocatalytic water splitting over the (BS)-Pt/TiO_2 catalysts, H_2 and O_2 were evolved via the reaction of $H_2O \rightarrow H_2 + 1/2O_2$. The gas evolution rates were *ca.* 5–10 times larger than those over the (PD)-Pt/TiO_2 catalysts.
(2) The TEM measurements showed that the deposited Pt particles were highly dispersed on the TiO_2 powder support by the polygonal barrel-sputtering method. The sizes of the deposited particles were smaller than those in the sample prepared by the photodeposition method. The deposition of the small Pt particles increased the Pt surface area, which contributed to the high water splitting activities of (BS)-Pt/TiO_2.
(3) The Pt particles deposited in (PD)-Pt/TiO_2 were the electron-rich Pt metals, while those in (BS)-Pt/TiO_2 were the electron-deficient Pt metals. These different electron states of the deposited Pt would mainly affect the water splitting activities of the Pt/TiO_2 catalysts.

Acknowledgment

This research was partially supported by JSPS KAKENHI Grant-in-Aid for Specially Promoted Research (JP16H06293), and Grant-in-Aid for Scientific Research (C) (JP18K05292).

References

[1] J. Nowotny, T.N. Veziroglu, Impact of hydrogen on the environment, Int. J. Hydrogen Energy 36 (2011) 13218–13224.
[2] K. Faungnawakij, R. Kikuchi, T. Matsui, T. Fukunaga, K. Eguchi, A comparative study of solid acids in hydrolysis and steam reforming of dimethyl ether, Appl. Catal. A Gen. 333 (2007) 114–121.
[3] M. Turco, G. Bagnasco, C. Cammarano, P. Senese, U. Costantino, M. Sisani, Cu/ZnO/Al_2O_3 catalysts for oxidative steam reforming of methanol: the role of Cu and the dispersing oxide matrix, Appl. Catal. B: Environ 77 (2007) 46–57.
[4] R.D. Parmar, A. Kundu, K. Karan, Thermodynamic analysis of diesel reforming process: mapping of carbon formation boundary and representative independent reactions, J. Power Sources 194 (2009) 1007–1020.
[5] X. Wang, N. Wang, M. Li, S. Li, S. Wang, X. Ma, Hydrogen production by glycerol steam reforming with in situ hydrogen separation: a thermodynamic investigation, Int. J. Hydrogen Energy 35 (2010) 10252–10256.
[6] A. Fujishima, K. Honda, Electrochemical photolysis of water at a semiconductor electrode, Nature 238 (1972) 37–38.
[7] Y.K. Kho, A. Iwase, W.Y. Teoh, L. Mädler, A. Kudo, R. Amal, Photocatalytic H_2 evolution over TiO_2 nanoparticles. The synergistic effect of anatase and rutile, J. Phys. Chem. C 114 (2010) 2821–2829.
[8] K. Maeda, Photocatalytic water splitting using semiconductor particles: history and recent developments, J. Photochem. Photobiol. C: Photochem. Rev. 12 (2011) 237–268.
[9] K. Maeda, K. Domen, Water oxidation using a particulate $BaZrO_3$-$BaTaO_2N$ solid-solution photocatalyst that operates under a wide range of visible light, Angew. Chem. Int. Ed. 51 (2012) 9865–9869.
[10] D. Jing, L. Guo, L. Zhao, X. Zhang, H. Liu, M. Li, S. Shen, Efficient solar hydrogen production by photocatalytic water splitting: from fundamental study to pilot demonstration, Int. J. Hydrogen Energy 35 (2010) 7087–7097.
[11] M. Kohno, T. Kaneko, S. Ogura, K. Sato, Y. Inoue, Dispersion of ruthenium oxide on barium titanates ($Ba_6Ti_{17}O_{40}$, $Ba_4Ti_{13}O_{30}$, $BaTi_4O_9$ and $Ba_2Ti_9O_{20}$) and photocatalytic activity for water decomposition, J. Chem. Soc. Faraday Trans. 94 (1998) 89–94.
[12] H. Kato, K. Asakura, A. Kudo, Highly efficient water splitting into H_2 and O_2 over lanthanum-doped $NaTaO_3$ photocatalysts with high crystallinity and surface nanostructure, J. Am. Chem. Soc. 125 (2003) 3082–3089.
[13] S. Onsuratoom, S. Chavadej, T. Sreethawong, Hydrogen production from water splitting under UV light irradiation over Ag-loaded mesoporous-assembled TiO_2–ZrO_2 mixed oxide nanocrystal photocatalysts, Int. J. Hydrogen Energy 36 (2011) 5246–5261.
[14] S. Sato, J.M. White, Photocatalytic water decomposition and water-gas shift reactions over NaOH-coated, platinized TiO_2, J. Catal. 69 (1980) 128–139.
[15] K. Sayama, H. Arakawa, Significant effect of carbonate addition on stoichiometric photodecomposition liquid water into hydrogen and oxygen from platinum-titanium(iv) oxide suspension, J. Chem. Soc. Chem. Commun. (1992) 150–152.
[16] S. Tabata, H. Nishida, Y. Masaki, K. Tabata, Stoichiometric phtocatalytic decomposition of pure water in Pt/TiO_2 aqueous suspension system, Catal. Lett. 34 (1995) 245–249.
[17] K. Sayama, H. Arakawa, Effect of carbonate salt addition on the photocatalytic decomposition of liquid water over Pt-TiO_2 catalyst, J. Chem. Soc. Faraday Trans. 93 (1997) 1647–1654.
[18] H. Arakawa, K. Sayama, Solar hydrogen production. Significant effect of Na_2CO_3 addition on water splitting using simple oxide semiconductors photocatalysts, Catal. Surv. Jpn. 4 (2000) 75–80.
[19] H. Kominami, S. Murakami, M. Kohno, Y. Kera, K. Okada, B. Ohtani, Stoichiometric decomposition of water by titanium(IV) oxide photocatalyst synthesized in organic media: effect of synthesis and irradiation conditions on photocatalytic activity, Phys. Chem. Chem. Phys. 3 (2001) 4102–4106.
[20] M. Kitano, K. Tsujimaru, M. Anpo, Hydrogen production using highly active titanium oxide-based photocatalysts, Top. Catal. 49 (2008) 4–17.
[21] H. Hata, Y. Kobayashi, V. Bojan, W.J. Youngblood, T.E. Mallouk, Direct deposition of trivalent rhodium hydroxide nanoparticles onto a semiconducting layered calcium niobate for photocatalytic hydrogen evolution, Nano Lett. 8 (2008) 794–799.
[22] N. Sakamoto, H. Ohtsuka, T. Ikeda, K. Maeda, D. Lu, M. Kanehara, K. Teramura, T. Teranishi, K. Domen, Highly dispersed noble-metal/chromia (core/shell) nanoparticles as efficient hydrogen evolution promoters for photocatalytic overall water splitting under visible light, Nanoscale 1 (2009) 106–109.
[23] K. Maeda, M. Higashi, D. Lu, R. Abe, K. Domen, Efficient nonsacrificial water splitting through two-step photoexcitation by visible light using a modified oxynitride as a hydrogen evolution photocatalyst, J. Am. Chem. Soc. 132 (2010) 5858–5868.
[24] H. Yamashita, K. Mori, Y. Kuwahara, T. Kamegawa, M. Wen, P. Verma, M. Che, Single-site and nano-confined photocatalysts designed in porous materials for environmental uses and solar fuels, Chem. Soc. Rev. 47 (2018) 8072–8096.
[25] M. Hara, Y. Hatano, T. Abe, K. Watanabe, T. Naitoh, S. Ikeno, Y. Honda, Hydrogen absorption by Pd-coated ZrNi prepared by using barrel-sputtering system, J. Nucl. Mater. 320 (2003) 265–271.
[26] T. Abe, S. Akamaru, K. Watanabe, Surface modfication of Al_2O_3 ceramic grains using a new RF sputtering system developed for powdery materials, J. Alloys Compd. 377 (2004) 194–201.
[27] T. Abe, S. Akamaru, K. Watanabe, Y. Honda, Surface modification of polymer microparticles using a hexagonal-barrel sputtering system, J. Alloys Compd. 402 (2005) 227–232.
[28] S. Akamaru, S. Higashide, M. Hara, T. Abe, Surface coating of small SiO_2 particles with TiO_2 thin layer by using barrel-sputtering system, Thin Solid Films 513 (2006) 103–109.
[29] T. Abe, H. Hamatani, S. Higashide, M. Hara, S. Akamaru, Surface coating of small SiO_2 particles with a WO_3 thin film by barrel-sputtering method, J. Alloys Compd. 441 (2007) 157–161.
[30] T. Abe, S. Higashide, M. Inoue, S. Akamaru, Surface modification of fine particles with a SnO_2 film by using a polyhedral-barrel sputtering system, Plasma Chem. Plasma Process. 27 (2007) 799–811.
[31] M. Inoue, H. Shingen, T. Kitami, S. Akamaru, A. Taguchi, Y. Kawamoto, A. Tada, K. Ohtawa, K. Ohba, M. Matsuyama, K. Watanabe, I. Tsubone, T. Abe, Preparation and physical and electrochemical properties of carbon-supported Pt–Ru (Pt–Ru/C) samples using the polygonal barrel-sputtering method, J. Phys. Chem. C 112 (2008) 1479–1492.
[32] H. Yamamoto, K. Hirakawa, T. Abe, Surface modification of carbon nanofibers with platinum nanoparticles using a “polygonal barrel-sputtering” system, Mater. Lett. 62 (2008) 2118–2121.
[33] M. Inoue, S. Akamaru, A. Taguchi, T. Abe, Physical and electrochemical properties of Pt–Ru/C samples prepared on various carbon supports by using the barrel sputtering system, Vacuum 83 (2009) 658–663.
[34] M. Inoue, T. Nishimura, S. Akamaru, A. Taguchi, M. Umeda, T. Abe, CO oxidation on non-alloyed Pt and Ru electrocatalysts prepared by the polygonal barrel-sputtering method, Electrochim. Acta 54 (2009) 4764–4771.
[35] T. Abe, M. Tanizawa, K. Watanabe, A. Taguchi, CO2 methanation property of Ru nanoparticle-loaded TiO2 prepared by a polygonal barrel-sputtering method, Energy Environ. Sci. 2 (2009) 315–321.
[36] K. Hirakawa, M. Inoue, T. Abe, Methanol oxidation on carbon-supported Pt–Ru and TiO_2 (Pt–Ru/TiO_2/C) electrocatalyst prepared using polygonal barrel-sputtering method, Electrochim. Acta 55 (2010) 5874–5880.
[37] C. Hiromi, M. Inoue, A. Taguchi, T. Abe, Optimum Pt and Ru atomic composition of carbon-supported Pt–Ru alloy electrocatalyst for methanol oxidation studied by the polygonal barrel-sputtering method, Electrochim. Acta 56 (2011) 8438–8445.
[38] S. Akamaru, M. Inoue, Y. Honda, A. Taguchi, T. Abe, Preparation of Ni nanoparticles on submicron-sized Al_2O_3 powdery substrate by polyhedral-barrel-sputtering technique and their magnetic properties, Jpn. J. Appl. Phys. 51 (2012) 065201.
[39] A. Taguchi, M. Inoue, C. Hiromi, M. Tanizawa, T. Kitami, T. Abe, Study of the surface morphology of platinum thin films on powdery substrates prepared by the barrel sputtering system, Vacuum 83 (2009) 575–578.
[40] A.M. Motin, T. Haunold, A.V. Bukhtiyarov, A. Bera, C. Rameshan, G. Rupprechter, Surface science approach to Pt/carbon model catalysts: XPS, STM and microreactor studies, Appl. Surf. Sci. 440 (2018) 680–687.
[41] J. Yu, L. Qi, M. Jaroniec, Hydrogen production by photocatalytic water splitting over Pt/TiO_2 nanosheets with exposed (001) Facets, J. Phys. Chem. C 114 (2010) 13118–13125.
[42] Z. Yi, W. Wei, S. Lee, G. Jianhua, Photocatalytic performance of plasma sprayed Pt-modified TiO_2 coatings under visible light irradiation, Catal. Commun. 2007 (8) (2007) 906–912.
[43] H.-J. Fan, C.-S. Lu, Lee W-LW, M.-R. Chiou, C.-C. Chen, Mechanistic pathways differences between P25-TiO_2 and Pt-TiO_2 mediated CV photodegradation, J. Hazard. Mater. 185 (2011) 227–235.
[44] A. Pozio, M. De Francesco, A. Cemmi, F. Cardellini, L. Giorgi, Comparison of high surface Pt/C catalysts by cyclic voltammetry, J. Power Sources 105 (2002) 13–19.
[45] T. Vidaković, M. Christov, K. Sundmacher, The use of CO stripping for in situ fuel cell catalyst characterization, Electrochim. Acta 52 (2007) 5606–5613.
[46] B. Sreedhar, D.K. Devi, D. Yada, Selective hydrogenation of nitroarenes using gum acacia supported Pt colloid an effective reusable catalyst in aqueous medium, Catal. Commun. 12 (2011) 1009–1014.
[47] E.A. Kozlova, T.P. Lyubina, M.A. Nasalevich, A.V. Vorontsov, A.V. Miller, V.V. Kaichev, V.N. Parmon, Influence of the method of platinum deposition on activity and stability of Pt/TiO_2 photocatalysts in the photocatalytic oxidation of dimethyl methylphosphonate, Catal. Commun. 12 (2011) 597–601.
[48] J. Ohyama, A. Yamamoto, K. Teramura, T. Shishido, T. Tanaka, Modification of metal nanoparticles with TiO_2 and metal-support interaction in photodeposition, ACS Catal. 1 (2011) 187–192.
[49] C.-H. Lin, J.-H. Chao, C.-H. Liu, J.-C. Chang, F.-C. Wang, Effect of calcination temperature on the structure of a Pt/TiO_2 (B) nanofiber and its photocatalytic activity in generating H_2, Langmuir 24 (2008) 9907–9915.
[50] J.C. Colmenares, A. Magdziarz, M.A. Aramendia, A. Marinas, J.M. Marinas, F.J. Urbano, J.A. Navio, Influence of the strong metal support interaction effect (SMSI) of Pt/TiO_2 and Pd/TiO_2 systems in the photocatalytic biohydrogen production from glucose solution, Catal. Commun. 16 (2011) 1–6.
[51] J.S. Jang, S.H. Choi, H.G. Kim, J.S. Lee, Location and state of Pt in platinized CdS/TiO_2 photocatalysts for hydrogen production from water under visible light, J. Phys. Chem. C 112 (2008) 17200–17205.
[52] G. Liu, H.Y. Gui, X. Wang, L. Cheng, H. Lu, L. Wang, Lu GQ(M), H.-M. Cheng, Enhanced photoactivity of oxygen-deficient anatase TiO_2 sheets with dominant {001} facets, J. Phys. Chem. C 113 (2009) 21784–21788.
[53] I. Lopez-Salido, D.C. Lim, R. Dietsche, B. Nils, Y.D. Kim, Electronic and geometric properties of Au nanoparticles on highly ordered pyrolytic graphite (HOPG) studied using X-ray photoelectron spectroscopy (XPS) and scanning tunneling microscopy (STM), J. Phys. Chem. B 110 (2006) 1128–1136.
[54] S. Garbarino, A. Pereira, C. Hamel, É Irissou, M. Chaker, D. Guay, Effect of size on the electrochemical stability of Pt nanoparticles deposited on gold substrate, J. Phys. Chem. C 114 (2010) 2980–2988.
[55] P. Marcus, C. Hinnen, XPS study of the early stages of deposition of Ni, Cu and Pt on HOPG, Surf. Sci. 392 (1997) 134–142.

[56] A. Howard, D.N.S. Clark, C.E.J. Mitchell, R.G. Egdell, V.R. Dhanak, Initial and final state eff ;ects in photoemission from Au nanoclusters on TiO_2(110), Surf. Sci. 518 (2002) 210–224.
[57] P. Zhang, T.K. Sham, X-ray studies of the structure and electronic behavior of alkanethiolate-capped gold nanoparticles: The interplay of size and surface effects, Phys. Rev. Lett. 90 (2003) 245502.
[58] E. Dilonardo, A. Milella, P. Cosma, R. d'Agostino, F. Palumbo, Plasma deposited electrocatalytic films with controlled content of Pt nanoclusters, Plasma Process. Polym. 8 (2011) 452–458.